A modular gradient-sensing network for chemotaxis in *Escherichia coli* revealed by responses to time-varying stimuli

Thomas S Shimizu[1,3], Yuhai Tu[2] and Howard C Berg[1,]*

[1] Department of Molecular and Cellular Biology, Harvard University, Cambridge, MA, USA and [2] T. J. Watson Research Center, IBM, Yorktown Heights, NY, USA
[3] Present address: FOM Institute for Atomic and Molecular Physics (AMOLF), Science Park 104, 1098 XG Amsterdam, The Netherlands
* Corresponding author. Department of Molecular and Cellular Biology, Harvard University, 16 Divinity Avenue, Cambridge, MA 02138, USA.
Tel.: +1 617 495 0924; Fax: +1 617 496 1114; E-mail: hberg@mcb.harvard.edu

The *Escherichia coli* chemotaxis-signaling pathway computes time derivatives of chemoeffector concentrations. This network features modules for signal reception/amplification and robust adaptation, with sensing of chemoeffector gradients determined by the way in which these modules are coupled *in vivo*. We characterized these modules and their coupling by using fluorescence resonance energy transfer to measure intracellular responses to time-varying stimuli. Receptor sensitivity was characterized by step stimuli, the gradient sensitivity by exponential ramp stimuli, and the frequency response by exponential sine-wave stimuli. Analysis of these data revealed the structure of the feedback transfer function linking the amplification and adaptation modules. Feedback near steady state was found to be weak, consistent with strong fluctuations and slow recovery from small perturbations. Gradient sensitivity and frequency response both depended strongly on temperature. We found that time derivatives can be computed by the chemotaxis system for input frequencies below 0.006 Hz at 22°C and below 0.018 Hz at 32°C. Our results show how dynamic input–output measurements, time honored in physiology, can serve as powerful tools in deciphering cell-signaling mechanisms.
Molecular Systems Biology **6**: 382; published online 22 June 2010; doi:10.1038/msb.2010.37
Subject Categories: signal transduction
Keywords: adaptation; feedback; fluorescence resonance energy transfer (FRET); frequency response; Monod–Wyman–Changeux (MWC) model

Introduction

Signaling networks are complex, but typically possess modular architectures (Hartwell *et al*, 1999). This observation provides hope for understanding the function of the whole in terms of simpler representations of its constituent parts. Much recent work on signaling networks has focused on assigning discrete functions to these parts; however, an essential next step is to determine the nature of the coupling between them.

Here, we have combined theoretical modeling with *in vivo* measurements of signaling to characterize the transfer functions of the two modules involved in computations of time derivatives by the *Escherichia coli* chemotaxis-signaling pathway. The first module, which we call the receptor module, detects changes in environmental conditions to generate an intracellular signal. This module has been shown to amplify signals over a wide dynamic range (Bray, 1998; Sourjik and Berg, 2002b). The second module, which we call the

adaptation module, is known to maintain the intracellular signal at a steady state that is indifferent to ambient concentrations of ligand (Berg and Tedesco, 1975; Spudich and Koshland, 1975; Barkai and Leibler, 1997; Alon *et al*, 1999). Both modules have been characterized extensively by experiment, and theoretical efforts to explain their behavior have enjoyed remarkable success. However, understanding how these modules combine in living cells to produce the biologically important function of gradient sensing requires additional knowledge about the way in which they are coupled *in vivo*.

To define this link quantitatively, we used a simple theoretical model of the chemotaxis pathway that abstracts many of the known molecular details, but preserves the essential characteristics of the receptor response and adaptation dynamics (Tu *et al*, 2008). We exploited an important result of this analysis that provides us with a method for inferring the dynamics of one module through input–output measurements of the other. Specifically, we used fluorescence

resonance energy transfer (FRET) to monitor the real-time activity of the sensory receptor–kinase complex, while subjecting cells to time-varying stimuli that render the output of this receptor module constant in time. Such a stimulus was identified by Block *et al* (1983), who found that the output, as inferred by the switching statistics of the flagellar motor, reached a steady value during exponential ramps, that is, ligand profiles that increase or decrease exponentially in time. Under these conditions, the feedback signal must exactly cancel the change in input signal, so we can infer the dynamics in the adaptation module through measurements of the receptor module, given a well-calibrated model of the latter and good control over the temporal profile of ligand input. Fortunately, the receptor module has been characterized in detail by a large body of *in vitro* experiments (Dunten and Koshland, 1991; Borkovich *et al*, 1992; Li and Weis, 2000; Bornhorst and Falke, 2001; Antommattei *et al*, 2004; Lai *et al*, 2005), *in vivo* FRET experiments (Sourjik and Berg, 2002b, 2004; Sourjik *et al*, 2007; Endres *et al*, 2008), and theoretical modeling (Shi and Duke, 1998; Duke and Bray, 1999; Mello and Tu, 2003, 2005, 2007; Shimizu *et al*, 2003; Mello *et al*, 2004; Sourjik and Berg, 2004; Keymer *et al*, 2006; Skoge *et al*, 2006). Our model uses a variant of the Monod–Wyman–Changeux (MWC) model for the receptor module, which we calibrated by measuring FRET responses to step stimuli in a series of adaptation-deficient mutants with systematically varying receptor-modification levels. This 'open-loop' transfer function of the receptor module defines quantitatively the way in which ligand concentration, the input signal, is balanced by receptor covalent modification, the feedback signal.

This model-driven approach provided two important advantages. First, we were able to measure the downstream adaptation dynamics through the same FRET method earlier developed to characterize the upstream receptor–kinase response (Sourjik *et al*, 2007). Second, because we measured the receptor module's output as a proxy for inferring the dynamics of the adaptation module, the measurement automatically yielded a second input–output relation, namely the response in adaptation kinetics to input from the receptor module. In short, we could elucidate the essential dynamical character of the downstream adaptation module without directly monitoring any of its molecular constituents.

In addition to ramp responses, we also measured responses to oscillatory input signals, which revealed the frequency response of the system. Together, these measurements allowed us to quantify two biologically important performance characteristics of the *E. coli* chemotaxis system, namely the output of time-derivative computations, and the frequency band over which such computations can be carried out. In contrast to earlier results obtained by monitoring motor switching statistics, no discontinuities in kinase activity were observed. Data collected at two different temperatures suggest a strong dependence of gradient-sensing performance on the ambient temperature.

Results

We present in Figure 1A a molecular view of the chemotaxis network, and in Figure 1B, the simplified view adopted in our
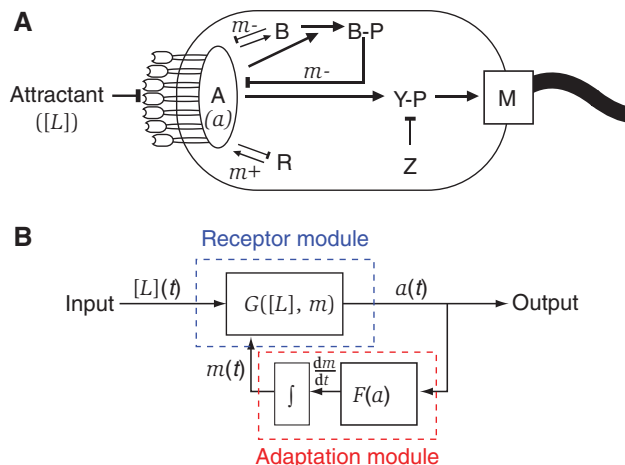
Figure 1 A modular gradient-sensing network. (**A**) Molecular view of the chemotaxis network. The linear path from input to output begins with the input ligand concentration, [*L*], being sensed by the membrane-associated receptor–kinase complex, *A*, to regulate its autophosphorylation-activity, *a*. *A* then transfers phosphate to the response regulator, CheY (*Y*), the phosphorylated form of which (*Y-P*) interacts with the flagellar motor (*M*), to control swimming behavior. The feedback loop is closed by the methyltransferase CheR (*R*) and the methylesterase/deamidase CheB (*B*), by regulation of the receptor methylation level, *m*. CheZ (*Z*), the phosphatase for CheY-P, decreases the signal lifetime, thus accelerating the response of the pathway. (**B**) Modular view of the network. Focusing on the functional modules, rather than the variables, of the network yields this block diagram, in which the variables are viewed as inputs or outputs (represented along wires) of two discrete signal processing modules (represented as boxes). The input–output relation of the receptor module is described by the function *G*, which takes [*L*] and *m* as inputs to produce an output *a*, which connects to the downstream linear pathway toward motor output. The adaptation module constitutes the feedback loop of the network, in which the output *a* is converted through *F*(*a*) to d*m*/d*t* and integrated over time.

model. At the molecular level, the intracellular signal pathway comprises multiple species of transmembrane receptors (also known as methyl-accepting chemotaxis proteins), a scaffolding protein CheW (not shown), the histidine kinase CheA, the response regulator CheY, its phosphatase CheZ, and the receptor-modification enzymes CheR and CheB. The phosphorylated form of CheY, CheY-P, is the final output of the intracellular pathway that directly interacts with the flagellar motor to modulate swimming behavior. The steady-state level of this signal is determined by the balance between production of CheY-P, catalyzed by CheA, and its destruction, catalyzed by CheZ. We denote the activity of the receptor–kinase complex by a, which is feedback regulated by the methyltransferase CheR and the methylesterase/deamidase CheB through the receptor methylation level, m. The latter is defined as the average number of methylated glutamyl residues per receptor monomer—each receptor has a fixed number of these sites subject to reversible modification by CheR and CheB; for the aspartate receptor Tar, there are four, so the maximum value per monomer $M \equiv \max(m) = 4$. Whereas the receptor–kinase-activity a is known to increase with m, that is $\partial a / \partial m > 0$, increased a in turn leads to up-regulation of CheB (Borczuk *et al*, 1986), which removes methyl groups, and down-regulation of CheR (Boldog *et al*, 2006), which adds methyl groups. Thus, the sense of the feedback is negative, tending to restore a toward its steady-state value on changes in the input ligand concentration, [*L*]. CheZ, the phosphatase for CheY-P,

decreases the signal lifetime, thus accelerating the response of the pathway. In our FRET assay, the energy transfer pair is CheY and CheZ, fluorescently labeled by genetic fusion to yellow fluorescent protein (YFP) and cyan fluorescent protein (CFP), respectively. The FRET signal is thus proportional to [CheY-P-CheZ], the concentration of the intermediate species in the enzymatic hydrolysis of CheY-P. At steady state, the production rate of CheY-P, catalyzed by CheA, is exactly balanced by its destruction rate, which is proportional to [CheY-P-CheZ]. Hence, the FRET signal serves as a readout of CheA kinase activity, the output of the receptor module.

In addition to the molecular constituents, we highlight in Figure 1A three important dynamical variables from this network, namely $[L]$, a, and m, which, respectively, correspond to the input, output, and feedback signals. We capture the dynamics of these variables in two simple equations:

$$\frac{\mathrm{d}m}{\mathrm{d}t} = F(a) \qquad (1)$$

$$a = G([L], m) \qquad (2)$$

As the receptor-modification reactions are much slower than all other reactions in the system, we model the rate of change of the feedback signal m explicity by a differential equation (equation (1)), and denote its dependence on the current signal output, a, by the function F. The receptor–kinase output, a, is known to relax much more rapidly (Sourjik and Berg, 2002a), and so its value at every instant is given by the algebraic equation (equation (2)), in which the function G denotes the dependence on the current ligand input, $[L]$, and feedback signal, m. Thus, equations (1) and (2) describe the adaptation and receptor modules, respectively. This two-module architecture is emphasized in the block diagram of Figure 1B, which clarifies the function of the two functions appearing in equations (1) and (2) within this signaling circuit: F is a transfer function contributing to the feedback gain of the network, whereas G combines the ligand input $[L]$ and the feedback signal m to produce the network output a. We use for G an allosteric model of the MWC type (Monod *et al*, 1965), in which the effects on kinase activity of both the ligand input $[L]$ and the feedback signal m contribute additively to the free-energy balance governing the two-state output of receptor–kinase complexes with N ligand-binding subunits.

The properties of the functions F and G would depend on details of the many molecular components, but, importantly, each has only one or two dynamical inputs and both have a single output. The integral sign appearing before F in Figure 1B signifies integral feedback (Yi *et al*, 2000), which is a well-known engineering design for robust adaptation, and is a direct consequence of equation (1): as the function F defines the feedback signal m's rate of change in time, m itself must be the time integral of F, that is $m(t) = \int F(a)\mathrm{d}t$. Thus, the function F is an important design feature of this signaling circuit, as it not only determines the dynamics of the feedback regulation (equation (1)), but also defines a crucial link between the two modules of the network: from the amplified output of the receptor module, to integral feedback in the adaptation module. Here, we experimentally probe this crucial link and quantitatively determine the feedback strength by measuring the response to time-varying stimuli *in vivo*.

Exponential ramps shift the steady-state kinase activity

We first confirmed that the kinase output during exponential ramps of the form $[L](t)=[L]_0 e^{rt}$ as measured by FRET reaches a constant steady-state level. To dynamically control the input $[L](t)$, we fabricated a mixing apparatus (described in Materials and methods) based on the design of Block *et al* (1983). Cells were first adapted to a baseline concentration, $[L]_0$, of the attractant α-methyl-DL-aspartate (MeAsp). The FRET signal was stabilized at $FRET_0$, although some fluctuations were unavoidable because of noise originating in the syringe-pump-driven injection of attractant to the mixing chamber. On applying both up ramps ($r>0$; Figure 2A, C, E, and G), and down ramps ($r<0$; Figure 2B, D, F, and H), the FRET signal was found to relax to a new, constant value, $FRET_c$, as expected. As the magnitude of this change, $\Delta FRET$ (expressed in arbitrary units), is proportional to the change in kinase-activity, Δa, and the latter, by definition lies on the unit interval, we can convert from FRET units to kinase-activity (a) units by measuring the full range of $\Delta FRET$. We obtain this by measuring the saturating values for $\Delta FRET$ in both directions, negative ($\Delta FRET_{sat}^-$) and positive ($\Delta FRET_{sat}^+$), by addition and removal of a large concentration of attractant, respectively. Thus, the pre-stimulus kinase activity $a_0=-\Delta FRET_{sat}^-/(\Delta FRET_{sat}^+-\Delta FRET_{sat}^-)$, the change in kinase activity $\Delta a=\Delta FRET/(\Delta FRET_{sat}^+-\Delta FRET_{sat}^-)$, and the constant kinase activity during exponential ramps $a_c=a_0 + \Delta a_c$.

Ramp responses determine the feedback function and the gradient sensitivity

The constant response in kinase-activity a_c that is reached during exponential ramps (Figure 2A–H) can be viewed as the output of time-derivative computations by the chemotaxis network. As the receptor module responds to the logarithmic change of the input signal (Tu *et al*, 2008; Kalinin *et al*, 2009), the relevant time derivative is that of the logarithm of input, that is $\mathrm{d}\ln[L]/\mathrm{d}t$, which corresponds in these experiments to the exponential ramp rate r. We therefore conducted exponential ramp-response measurements of the type depicted in Figure 2A and B over a range of ramp rates r. The asymptotic kinase response, a_c, obtained through such measurements, is plotted in Figure 3A as a function of r. The steady-state activity in the absence of stimuli (i.e. at $r=0$) was found to be $a_0 \approx 1/3$. This plot reveals the sensitivity of *E. coli* to temporal gradients of MeAsp, and the overall shape is sigmoidal, with a steep slope ($\Delta a_c/\Delta r \approx -30$ s) near $r=0$. This implies that the system is tuned to respond sensitively to very shallow gradients, but it has a relatively narrow dynamic range: at greater absolute ramp rates, it becomes largely insensitive to changes in the gradient. If we define the slope $\Delta a_c/\Delta r$ as the gradient sensitivity, its value is large and nearly constant in the small interval near $r=0$, but decays rapidly outside of it. Importantly, we observed no response thresholds at small ramp rates (Figure 3A, inset), in contrast to Block *et al* (1983), in which it was found that the ramp-response magnitude reached zero at low ramp rates ($r\approx 0.005$ for up ramps, $r\approx 0.01$ for down ramps).
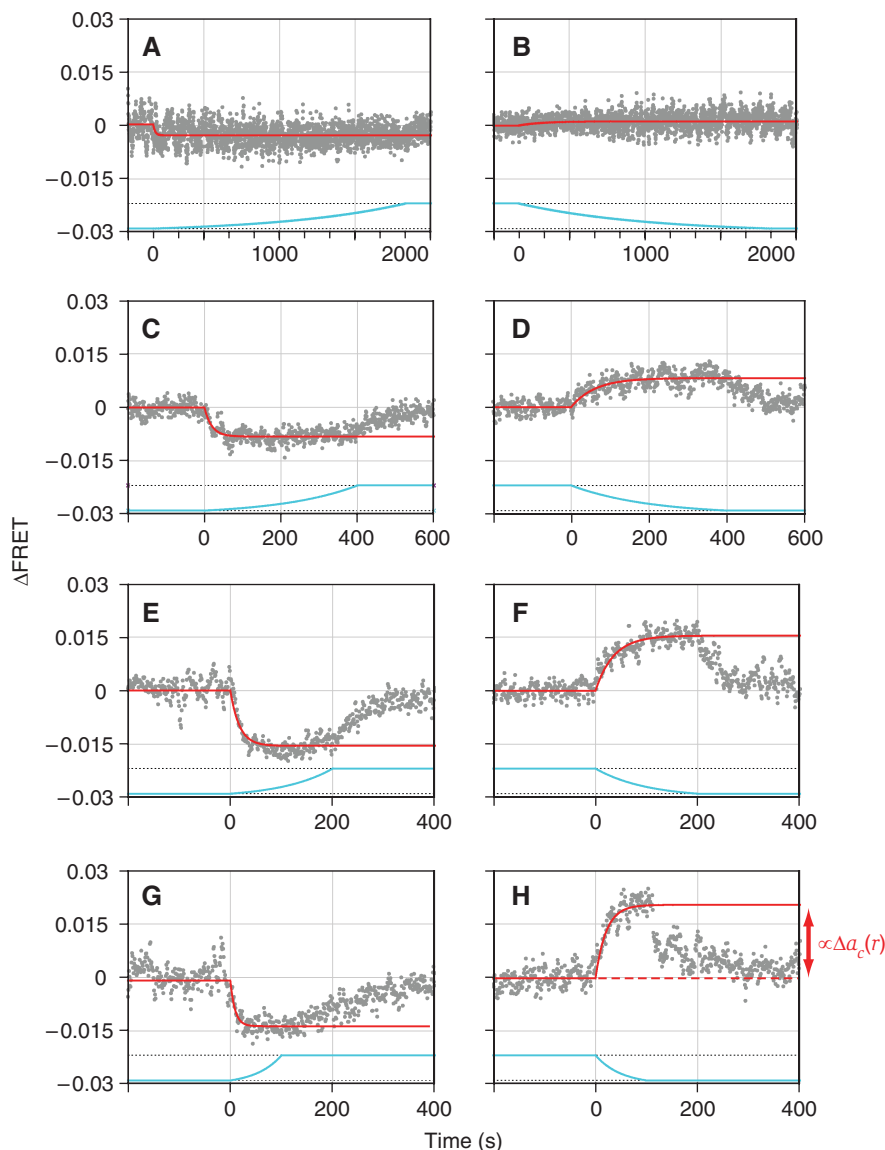
Figure 2 Temporal profiles of pathway activity during exponential ramps. FRET responses (gray points) were observed during stimulation by exponential ramps in concentration of the form $[L](t)=[L]_0 e^{rt}$ of the attractant MeAsp (blue curves). Responses were quantified by fitted functions to the FRET response (red curves). For both ramps up ($r>0$; **A**, **C**, **E**, **G**) or down ($r<0$; **B**, **D**, **F**, **H**), the FRET readout reached a steady level after an initial transient, which was well fit by a single-exponential decay. The change in the level of FRET could be converted to units of kinase activity, Δa (see text), which was negative for up ramps, and positive for down ramps, as expected. The traces in the panels here were responses to ramp rates $r=\pm 0.001$ (A, B), $r=\pm 0.005$ (C, D), $r=\pm 0.01$ (E, F), and $r=\pm 0.02$ (G, H). The gray points in each panel are aligned averages of two to three separately measured responses to identical stimuli. Source data is available for this figure at www.nature.com/msb.

The data of Figure 3A can be used further to infer the shape of the feedback transfer function $F(a)$. The recorded values of a_c are the outputs of the receptor module at which the effects of the time-varying ligand input, $[L](t)$, and that of the adaptation feedback, $m(t)$, are canceling one another exactly. Therefore, given a model of how these signals are processed within the receptor module, that is if we know the form of the function $G([L], m)$, we can infer the rate of change of the feedback signal, that is $dm(t)/dt=F(a)$, from the temporal input profile $[L](t)$ that is being cancelled. For an MWC-type receptor module experiencing exponential ramp stimuli, one can show (see Materials and methods) that cancellation of the ligand- and methylation-dependent free energy yields

$df_L/dt + df_m/dt = r - \alpha F(a_c) = 0$, where $\alpha \equiv -df_m/dm$ is the free-energy change per added methyl group (in units of kT). Thus, we can rescale the abscissa of Figure 3A to render it a reading of $F(a_c)=r/\alpha$, and invert the axes about the point ($r=0$, $a_c=a_0$) to obtain a plot of $F(a)$ (Figure 3B). The slope near the fixed point, $F'(a_0) \approx -0.01$, is negative and shallow, implying weak negative feedback.

Frequency–response measurements reveal the time-derivative computation and its bandwidth

Although the asymptotic gradient sensitivity (Figure 3A) can be viewed as the output of a time-derivative computation,
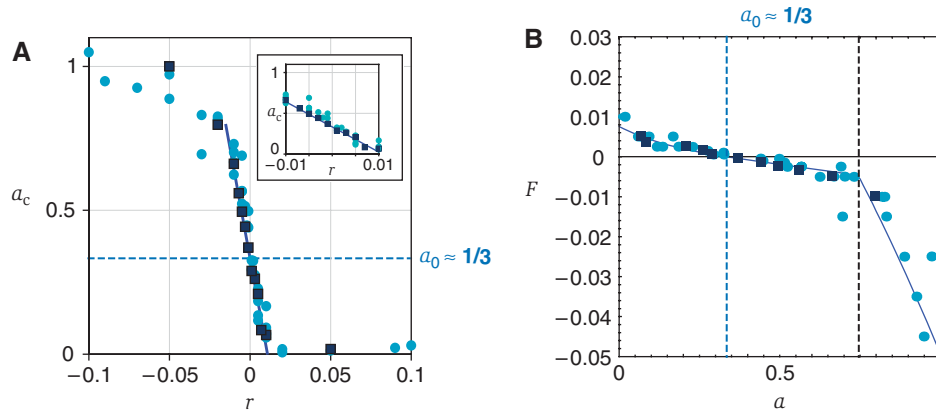
Figure 3 Gradient sensitivity and the feedback transfer function $F(a)$. (**A**) By measuring exponential ramp responses in the manner of Figure 2A–H over a range of ramp rates r, we constructed a gradient-sensitivity curve, relating the kinase-activity a, to the steepness of the temporal gradient experienced by cells. The results for two FRET strains considered wild type for chemotaxis (VS104, an RP437 derivative, cyan circles; TSS178, an AW405 derivative, dark blue squares) were essentially identical, and collapsed on to a sigmoidal curve with a steep region near $r=0$ (slope of fitted line, $\Delta a/\Delta r \approx -30$ s). The steady-state activity in the absence of stimuli (i.e. at $r=0$) was found to be $a_0 \approx 1/3$. The inset in (A) is an expanded view about the point ($r=0$, $a=a_0$), showing the absence of thresholds, at least down to $r=\pm 0.001$ s^{-1}. (**B**) Using our model, the data of (A) can be used to map the feedback transfer function $F(a)$. The steady-state relation $r=\alpha F(a_c)$ implies that we can rescale the r axis by the constant factor α, obtained from our calibration of the receptor-module transfer function G, and invert the axes about ($r=0$, $a=a_0$) to obtain $F(a)$. The shallow slope near this origin, $F'(a_0) \approx -0.01$, implies weak negative feedback. The blue curve is a fit of a Michaelis–Menten reaction scheme $F(a) = V_R \frac{1-a}{1-a+K_R} - V_B(a)\frac{a}{a+K_B}$; see text for interpretation of parameters. Source data is available for this figure at www.nature.com/msb.

it does not address what happens if such gradients change over time. For a swimming bacterium in the real world, gradients will rarely be constant, so how rapidly the cell can respond to changing gradients will also be important. We therefore measured the frequency response of the network by measuring responses to oscillatory stimuli $[L](t)=[L]_0 e^{A_L \sin(2\pi\nu t)}$ over a range of input frequencies, ν (Figure 4A). For small modulation amplitudes A_L, the response in FRET, converted again to receptor–kinase-activity units, was always found to be well fit by a sinusoid of the form $a(t)=a_0 + |A|\cos(2\pi\nu t - \varphi_D)$, where the frequency ν always matched that of the input modulation, whereas the response amplitude $|A|$ and phase delay φ_D were found to depend on ν (see below). This is the expected linear response to sine-wave modulation, consistent with the notion that the receptor module takes the logarithm of ligand concentration (Tu *et al*, 2008).

The measured frequency dependence of the response amplitude, $|A|$, and phase delay, φ_D, are plotted as points in Figure 4B and C. Given the measured value for $F'(a_0)$ obtained in our ramp experiments, our model can be used to determine the dependence of $|A|$ and φ_D on frequency. These predictions, shown as solid curves in Figures 4B and C, are in excellent agreement with the data. This solution yields a characteristic frequency ν_m defining the upper limit of the frequency band over which the system is able to take time derivatives. Using the measured parameters $a_0 \approx 1/3$ and $F'(a_0) \approx -0.01$ from our ramp-response measurements above, and $N=6$, $\alpha=2$ from our calibration of the receptor module, G (see Materials and methods), we obtain $\nu_m \approx 0.006$ Hz. By appropriate factoring of our model solution (see Materials and methods), we also obtain a function $|H|$, the chemotaxis system's filtering properties for the time derivative of the input signal (Figure 5B, green dashed curve). The shape of $|H|$ clarifies the low-pass property of this network for the derivative signal: the derivative signal is passed most efficiently below ν_m, in which the phase delay φ_D approaches $\pi/2$.

Temperature affects both gradient sensitivity and frequency response

All of the above measurements were made at room temperature (22°C) for consistency with earlier *in vivo* FRET studies (Sourjik and Berg, 2002b, 2004), but the earlier results of Block *et al* (1983) were obtained at the higher temperature of 32°C. For comparison, therefore, we also collected ramp- and frequency–response data at 32°C. Interestingly, the gradient sensitivity (Figure 5A) was attenuated at this higher temperature, and the slope near a_0 ($\approx 1/2$ at 32°C) was reduced to $\Delta a/\Delta r \approx -11$ s. To compare this with the gradient sensitivity found by Block *et al* (1983), we must convert our response, Δa, measured in kinase-activity units, into $\Delta\langle CCW \rangle$, the response in counter-clockwise-rotational bias of the flagellar motor. Using a Hill function $\langle CCW \rangle = 1/(1 + (a/K)^{n_H})$ for the motor response with $n_H=10$ (Cluzel *et al*, 2000), we find $\Delta\langle CCW \rangle/\Delta r = \frac{\partial\langle CCW \rangle}{\partial a}(\Delta a_c/\Delta r) \approx 55$ s, which is within $\sim$threefold of the Block *et al* result ($\Delta\langle CCW \rangle/\Delta r \approx 20$ s). However, no response thresholds were observed, even at this higher temperature (Figure 5A, inset). By the same procedure used to obtain Figure 3B from 3A, we can convert the gradient-sensitivity data of Figure 5A to obtain the shape of the feedback transfer function $F(a)$ at 32°C (Figure 5B). The frequency response of the system was also tested at 32°C using exponential sine-wave stimuli, and was again found to match closely the model prediction with $\nu_m \approx 0.018$, based on the slope $F'(a_0) \approx -0.03$ measured at this temperature.

The shape of the gradient response (Figure 5A) obtained from our FRET experiments contrasts strongly from that obtained by Block *et al* (1983) through motor-rotation measurements, in which a flat profile near $r=0$ had suggested the existence of response thresholds at small values of r. These differences remain unexplained, but we speculate that they are attributable to either or both of the following: (a) the difference in the output that has been measured; whereas we have
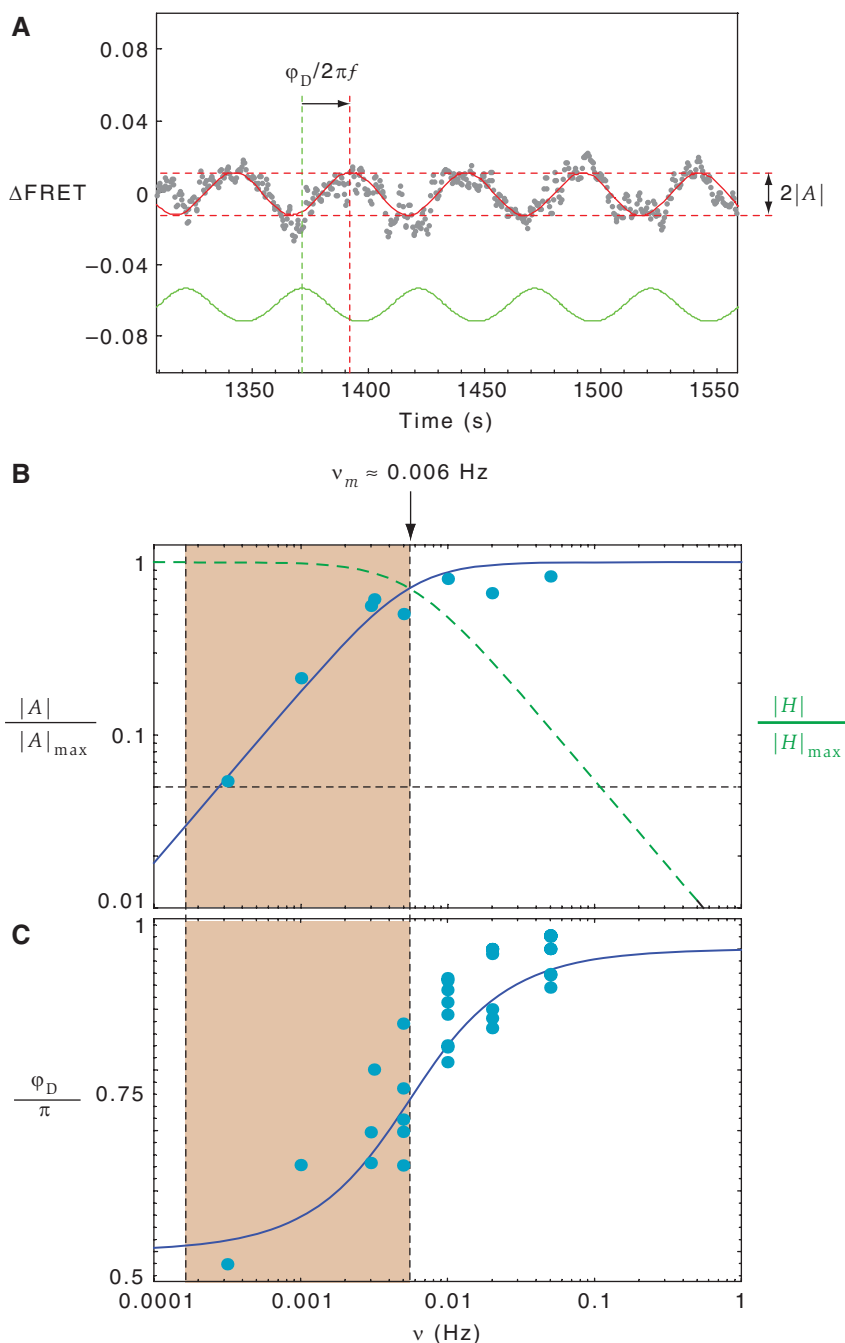
Figure 4 Frequency response and the bandwidth for derivative computations. FRET responses (gray dots) during stimulation by exponential sinusoids of the form $[L](t) = [L]_0 e^{A_L \sin(2\pi v t)}$ (**A**) with a frequency v equal to that of the applied stimulus (green line), and the fit by a sinusoid (red line) of the form $a(t) = a_0 + |A| \cos(2\pi v t - \varphi_D)$, where $|A|$ is the amplitude of the response and φ_D is the phase delay. When the amplitude (**B**) and phase (**C**) of responses are plotted against the driving frequency v, the data are in excellent agreement with the analytical solutions of our model (equations (13) and (14)), plotted here without any free-fitting parameters—the solution uses parameters obtained separately from the ramp-response experiments of Figure 2 and 3 and MWC-model parameters obtained separately in dose–response experiments using step stimuli. These analytical solutions define the characteristic frequency of the response $v_m \approx 0.006$ Hz, below which the network is able to compute time derivatives. The dashed green curve in (B) is the derivative-filtering function $|H|$ obtained by factoring the solution of our linearized model (equation (15)). The characteristic frequency, v_m determines the upper boundary of the frequency band over which time derivatives can be computed (shaded region). Presumably, the lower boundary would be determined by a noise floor, which in this figure is taken arbitrarily to be where the response amplitude (black curve in B) falls below 5% of maximum. Source data is available for this figure at www.nature.com/msb.

measured the kinase output by FRET between CheY and CheZ, Block *et al* (1983) measured the motor response, or (b) the amount of data collected in the two studies; whereas our FRET technique has allowed us to efficiently collect a relatively large

number of data points, each averaged over hundreds of cells (59 data points, each representing an average over hundreds of cells), the gradient response of Block *et al* (1983) was obtained using only a few cells (26 data points from 3 cells). The
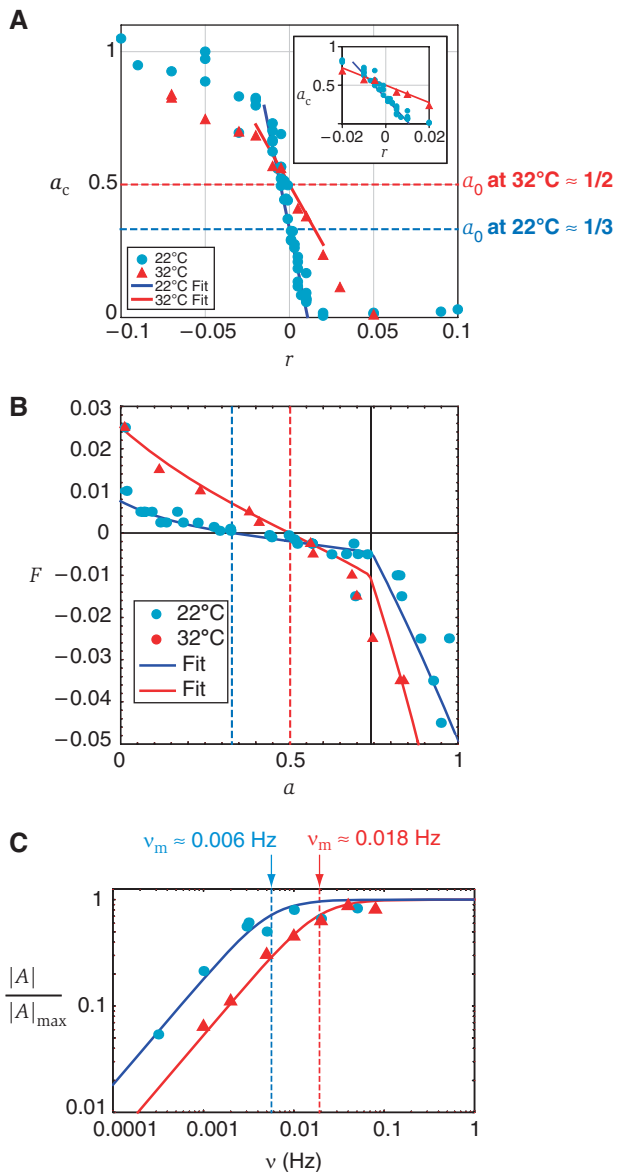
Figure 5 Effects of temperature on sensitivity to gradients and frequency response. (**A**) Sensitivity to gradients was markedly decreased at 32°C (red triangles; strain TSS178), in which the steady-state activity $a_0 \approx 1/2$. For comparison, the data at 22°C (same as Figure 3A) also are plotted (cyan circles; strains VS104 and TSS178). The slope of the linear fit to the 32°C points near a_0 (red curve) was $\Delta a/\Delta r \approx -11$ s. (**B**) The map of $F(a)$ obtained by conversion of the data in (A) has a similar shape as that at 22°C, but the slope at the zero crossing, $F'(a_0) \approx -0.03$, is approximately threefold steeper, implying stronger negative feedback. The red curve is a fit to the same Michaelis–Menten model as in Figure 3B (see text for parameter values and interpretation). (**C**) The frequency response is also shifted at 32°C (red triangles). The characteristic cutoff frequency $\nu_m \approx 0.018$, obtained from the model fit (black curve), is approximately threefold higher than that at 22°C. For comparison, the 22°C data and the corresponding model prediction from Figure 4A also are reproduced here (cyan circles and blue curve). Source data is available for this figure at www.nature.com/msb.

dependence of motor switching on [CheY-P] was found by Cluzel *et al* (2000) to be monotonic, steep, and highly reproducible between separately tested individual motors; therefore, there does not seem to be any way in which the continuous variation in [CheY-P] measured by FRET can give

rise to a discontinuous motor response. Thus, (b) seems to be the most plausible explanation.

Discussion

We have measured the dynamical response of *E. coli*'s chemotactic gradient-sensing circuit to time-varying chemical stimuli. Our results reveal this signaling network's sensitivity to temporal gradients, as well as its frequency-filtering properties. Using an important relationship identified by theoretical analysis (Tu *et al*, 2008), we derived from our exponential ramp-response measurements the feedback transfer function $F(a)$, which couples the two modules of this signaling pathway and reveals the dynamics of the adaptation module. Responses to oscillatory stimuli, the power of which has been exemplified in a number of recent studies (Bennett *et al*, 2008; Hersen *et al*, 2008; Mettetal *et al*, 2008), were used to characterize the frequency response of the pathway, which determines the frequency band over which the chemotaxis system can compute time derivatives (Andrews *et al*, 2006). We found the characteristic frequency of the adaptation system to depend on temperature, but it is in general compatible with weak feedback and large noise amplitudes at steady state. The use of time-varying stimuli allowed us to probe these dynamical characteristics of the adaptation module without direct measurement of the underlying biochemical reactions of receptor methylation/demethylation. This general approach of combining theory with experiment to probe the dynamics of pathway components not directly accessible to experiment should be applicable to many systems, and aid in the effort to uncover the design principles of biological circuits (Alon, 2007). We discuss here the implications of our findings in the context of earlier studies, and highlight possible directions for future work.

Effects of cell-to-cell variability: measurements in single cells and populations

A crucial difference between the measurements reported here and those of Block *et al* (1983) is that our FRET signals are collected simultaneously from hundreds of cells, whereas Block *et al* recorded the motor response of individual tethered bacteria. Although our data have much higher signal-to-noise ratios than the stochastic binary time series collected in the motor-response experiments, it is pertinent to ask whether the population-averaged nature of our FRET measurements might account for some of the differences in our observations. In particular, a striking difference was found in the exponential ramp responses to very shallow gradients (Figure 3A, inset); whereas Block *et al* could not detect responses to ramp rates in the interval $r \in (-0.01, +0.005)\,\mathrm{s}^{-1}$, no such thresholds were found in the exponential ramp responses we measured by FRET. Could this difference arise from ensemble averaging the output of individual cells, which individually possess such response thresholds?

We argue here that this is not possible if the typical single cell does indeed possess such response thresholds at the level of the receptor–kinase response. In the context of our preceding analyses, the qualitative question of threshold

existence can be recast as a quantitative one of gradient sensitivity: does there exist a region of negligible gradient sensitivity at very low ramp rates ($\Delta a_c / \Delta r \approx 0$ near $r=0$)? To make the distinction between individuals and populations explicit, we denote by $a_c^i(r)$ the steady-state activity of each individual cell in a population during an exponential ramp with rate r, and by $\langle a_c \rangle (r)$ the population-averaged activity we measure by FRET. As the latter is just a linear combination of single-cell activities, $\Delta \langle a_c \rangle (r) = \frac{1}{N_{cells}} \sum \Delta a_c^i(r)$, where N_{cells} is the number of cells in the population, the gradient sensitivity at the population level is just the average of the single-cell gradient sensitivities $\Delta \langle a_c \rangle / \Delta r = \frac{1}{N_{cells}} \sum_i \Delta a_c^i / \Delta r$. Thus, if the majority of cells possess response thresholds, this should have been evident in our population measurements.

Transient time of ramp responses: inference of cooperativity from dynamics

The gradient sensitivity, which we defined using the constant kinase-activity a_c reached during exponential ramps, can be viewed as the output of time-derivative computations by the chemotaxis system. Remarkably, the solution for this output in our model, $a_c = F^{-1}(r/\alpha)$, is independent of the parameter N, which represents the degree of receptor cooperativity in the MWC model. Thus, although receptor interactions have an amplifying function in the open-loop response to step and impulsive stimuli (Sourjik and Berg, 2004; Keymer *et al*, 2006; Mello and Tu, 2007; Tu *et al*, 2008)—the property traditionally referred to as the 'gain' of the chemotaxis system (cf. e.g. Segall *et al*, 1986)—the amplitude of responses to sustained temporal gradients is dictated only by the adaptation system (through the function $F(a)$). This does not mean, however, that receptor cooperativity is unimportant within the 'closed-loop' control structure of the chemotactic gradient-sensing circuit.

The function of receptor coupling becomes clear when one considers the time required for the chemotaxis network to take this time derivative, which is an equally important measure of performance for this gradient-sensing system. Our model provides a basis for investigating the molecular parameters that determine the speed of this computation, and yields the following simple, approximate expression for the time, t_1, required for the kinase activity to reach a_c during exponential ramps:

$$t_1 \approx \Delta f(a_c)/Nr \qquad (3)$$

where $\Delta f(a_c)$ is the free energy difference between the steady states with and without the ramp: $\Delta f(a_c) = \ln(1/a_c - 1) - \ln(1/a_0 - 1)$. The quantity $\Delta f(a_c)/N$ can be intuitively understood as a characteristic amount of chemical work that the adaptation system must perform before it can catch up with the rate r at which the ligand concentration is being ramped.

In the limit of shallow ramps (small r), where Δa_c is small, we can linearize equations (1) and (2) to solve for a limiting, minimum response time, $t_1 \rightarrow \tau_m = (-\alpha N a_0 (1-a_0) F'(a_0))^{-1} = (2\pi\nu_m)^{-1}$, where ν_m is the characteristic frequency of the linear response to oscillatory stimuli (see equation (14) of Materials and methods). This solution is independent of the applied (small) ramp rate r. At greater ramp rates, the linear approximation is no longer valid, but we can still estimate t_1 by the simple relation presented in equation (3). The justification for this approximation is illustrated in Figure 6A, which is a plot of the time course of the two free-energy contributions to kinase activity, stemming from ligand binding (f_L) and methylation (f_m). When an exponential ramp with rate r is started at $t=0$, f_L begins to rise immediately as $\sim rt$. The methylation-dependent contribution, $-f_m$, 'lags' behind f_L, but this lag asymptotically stabilizes as the methylation rate $F(a)$ reaches r/α, from which point on, the free-energy lag
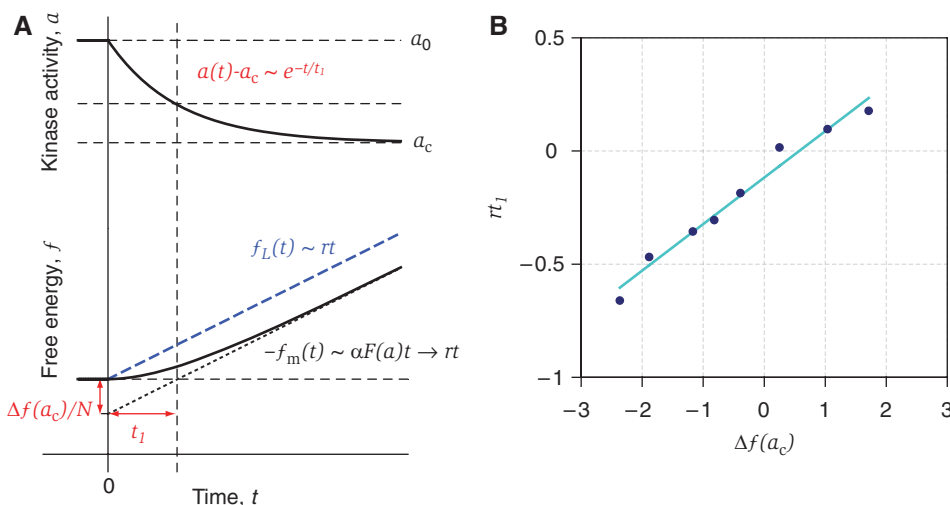
Figure 6 Transient responses to ramps: the time required for derivative computations. (**A**) Schematic illustration of the changes in activity and free energies during exponential ramps. As the receptor–kinase activity approaches the constant value a_c during exponential ramps, the rate of change of ligand- and methylation-dependent free energies (f_L and f_m, respectively) balance one another, leading to the asymptotic relation $r=\alpha F(a_c)$ between the exponential ramp rate r and the net rate of change in intracellular methylation $F(a)$ (see also Materials and methods). The time required for $f_m(t)$ to change by an amount equal to the total free-energy change $\Delta f(a_c)$ can be estimated as $t_1 \approx \Delta f(a_c)/Nr$, and provides a robust estimate for the time required for the activity $a(t)$ to reach a_c (see text). (**B**) A plot of rt_1 versus $\Delta f(a_c)$ for exponential ramp responses at 22°C. The slope of the fitted curve yields an estimate for the extent of receptor cooperativity, $N \approx 4.9$, which is in good agreement with the value of $N=6$ obtained independently from dose–response curves from experiments using step stimuli (see text).

$\Delta f(a)$, and hence the kinase activity become constant (i.e. $\Delta f(a) \to \Delta f(a_c)$, as $a(t) \to a_c$).

In the linear regime in which the transient time is independent of r, $a(t)$ will decay exponentially in time as $\sim e^{-t/t_1}$ toward a_c, and equation (3) is exact. The constant solution $t_1 = \tau_m$ in this case can be obtained by letting $r = \alpha F'(a_0)(a_c - a_0)$ in equation (3) and taking the limit $a_c \to a_0$. In the more general case, t_1 will not be independent of r, but equation (3) still provides a useful approximation. In particular, it retains the correct scaling with the extent of receptor cooperativity, N. To compute the points in Figure 6B, t_1 was estimated by fitting an exponential decay function of the form $a(t) = a_c + (a_0 - a_c)e^{-t/t_1}$ to the FRET data recorded during exponential ramp stimuli (such as those of Figure 2) at different values of r, and $\Delta f(a_c)$ was computed from the a_0 and a_c values from the same measurement.

As $\Delta f(a_c)$ is independent of the degree of receptor cooperativity, N, we can use equation (3) to extract from our experimental data an estimate for the parameter N. Although it recently has been reported (Endres *et al*, 2008) that the degree of receptor cooperativity seems, under certain conditions, to depend on the modification level of receptors (i.e. that N could depend on m, which is changing during our ramp measurements), the fact that we observe a constant activity during exponential ramps suggests that such changes in the organization of the receptor complex occur on time scales considerably slower than that of our time-varying stimuli. We, therefore, apply equation (3) to infer a single value of N from the set of t_1 values extracted from our ramp-response data. Although accurate determination of t_1 is difficult, because its estimation is more sensitive to experimental noise, the approximate linear scaling of the product $rt_1 \sim N^{-1} \Delta f(a_c)$ follows immediately from equation (3), and is more robust to noise than t_1 itself

(as the factor r conveniently diminishes the error more strongly in which Δa_c is small, and errors in estimating t_1 tend to be large). In Figure 6B, we plot rt_1 against $\Delta f(a_c)$, in which the slope of the fitted line gives an estimate $N \sim 4.9$, which is in satisfactory agreement with the more reliable value of $N = 6$, estimated through fits to dose–response curves to step stimuli (Mello and Tu, 2007; see also Materials and methods and Figure 7).

Biochemical interpretation of $F(a)$: enzyme saturation and CheB activation

The steady-state identity $r = \alpha F(a_c)$ derived from our model allowed us to map the feedback transfer function $F(a)$ from the gradient-response data measured at each temperature. We found that $F(a)$ is a nonlinear, monotonically decreasing function with a shallow slope near the steady-state fixed point, $F(a_0) = 0$, and a much steeper slope near the high-activity extreme, $F(1)$. As $F(a)$ represents the net rate of change of

Figure 7 Calibration of the receptor-module transfer function, $G([L],m)$. (**A**) FRET responses in kinase activity (points) to step stimuli of the attractant MeAsp were measured in a series of mutants in which the modification state of Tar receptors were fixed by deletions of the *cheR* and *cheB* genes. To reveal the response of the Tar receptor, these measurements were conducted in a genetic background in which Tsr and Tap receptors are not expressed. Fits to the allosteric MWC model (equations (6)–(8), with parameters $N=6$, $K_I/K_A=0.0062$ are shown as solid lines. The gray level of the points and solid curves indicate the modification state of the mutant strain, and is tabulated in the legend (lighter shades of gray for higher modification levels). The blue points and curve, denoted *wt* in this figure, is the strain VS178, which has the same receptor complement as the other mutants (Tsr−Tap−), but retains the wild-type genes for CheR and CheB. Kinase activity is shown normalized to the pre-stimulus value for the strain VS104. (**B**) Values of f_m, obtained for each modification state represented in (A), plotted against the number of modified sites. The data for modification states containing only glutamate (E) and glutamine (Q) residues (black points) fell on a straight line (dotted) when plotted as a function of the number of E→Q transitions ($n_{E \to Q}$; black points). The data for modification states containing only Q's and methylated glutamates (Em) fell on a different straight line (dashed), when plotted as a function of the number of Q→Em transitions ($n_{Q \to Em}$; magenta points). The values for the two extreme methylation levels, EEEE (corresponding to $m=0$) and EmEmEmEm (corresponding to $m=4$), were obtained by extrapolation of the two straight lines, as they could not be obtained directly from fits to the FRET data (cells with the Tar population fixed in this state did not respond to any concentration of MeAsp, as is seen in (A)). The solid line connecting these two extreme states reveals the dependence of f_m on the E→Em transitions ($n_{E \to Em}$; gray points), and the CheR+CheB+ strain VS178 (blue point, denoted *wt*) falls on this line, as expected. When fitted by equation (9), this line yields the parameters $m_0 \approx 0.5$ and $\alpha \approx 2\,kT$ used throughout this study. Source data is available for this figure at www.nature.com/msb.
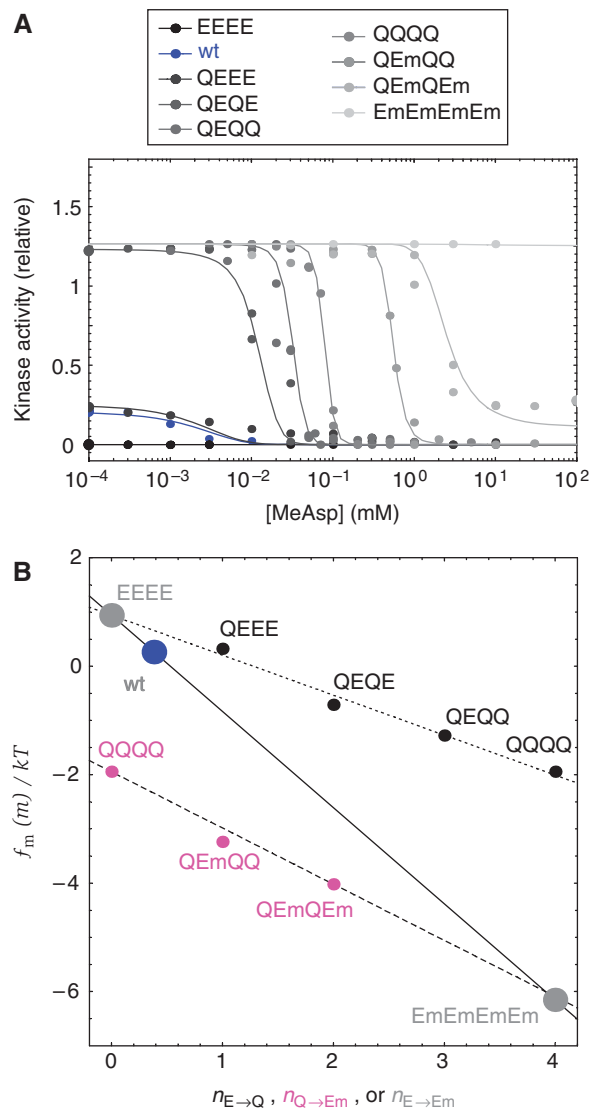
methylation catalyzed by CheR and CheB, a biochemical interpretation of this curve can be obtained by an enzymatic reaction model,

$$F(a) = V_R \frac{1-a}{K_R + 1 - a} - V_B(a) \frac{a}{K_B + a} \qquad (4)$$

where K_R and K_B are the Michaelis constants for each reaction, and V_R and $V_B(a)$ represent the velocities of the methylation and demethylation reactions, respectively, when those enzymes are saturated with substrate (all concentrations are normalized, in units of the CheA kinase concentration; for example $K_{R,B}$ are dimensionless, $V_{R,B}$ have units s^{-1}). This expression assumes that CheR can only bind the inactive fraction and CheB can only bind the active fraction of receptor–kinase complexes. Our measurements place strict limits on these end point values, $F(0)$ and $F(1)$. In our ramp-response data, $F(0)$ can be inferred from the ramp rate r_c at which the response amplitude to positive ramp-stimuli saturates (i.e. in which a_c reaches zero) by the relation $r_c = \alpha F(0)$. Reading off values for r_c from Figure 5B, and using again $\alpha = 2$ from our receptor-module calibration (described in Materials and methods), we expect $F(0) \approx 0.01$ at 22°C and $F(0) \approx 0.025$ at 32°C. The data are noisier at the opposite extreme of activity, but an approximate lower bound for the absolute value of $F(1)$ can readily be inferred by examining the maximal absolute response observed, which yields $|F(1)| > \sim 4F(0)$ at both temperatures. These constraints, combined with the high curvature near $F(1)$ and the location of a_0, precluded a fitting with a constant value for V_B. Evidently, what is required is a sharp increase in $V_B(a)$ as a approaches unity. The solid curves shown in Figures 3B and 5B use a simple piece-wise linear form, $V_B(a) = V_B(0)(1 + \theta(a - a_B) \frac{a - a_B}{1 - a_B} r_B)$, where $\theta(x)$ is the unit step function ($\theta(x) = 1$ for $x > 0$, $\theta(x) = 0$ otherwise), a_B represents the value of a above which a $V_B(a)$ increases, and r_B determines the maximum value of $V_B(a)$. For the data of Figure 5B, we found that $a_B = 0.74$ yields good fits for data at both temperatures. Values for other parameters are as follows: at 22°C, $\{V_R, V_B(0)\} = \{0.010, 0.013\}$ s^{-1}, $\{K_R, K_B\} = \{0.32, 0.30\}$, and $r_B = 4.0$; at 32°C, $\{V_R, V_B(0)\} = \{0.030, 0.030\}$ s^{-1} and $\{K_R, K_B\} = \{0.43, 0.30\}$, and $r_B = 2.7$.

The comparison between the two sets of experiments offers some insight regarding the temperature dependence of the parameters. The dominant difference is in the saturating velocities for methylation and demethylation, V_R and $V_B(a)$, which can be interpreted as the product of the active enzyme concentration and the catalytic rate constant k_{cat}. As the growth conditions before the experiments were identical, and measurements were conducted in a medium that does not support protein synthesis, the expression levels of enzymes were the same in the experiments at 22 and 32°C. Thus, we conclude that k_{cat}'s for methylation and demethylation are the parameters most sensitive to temperature in the adaptation system.

The mechanism responsible for the strongly nonlinear behavior of $V_B(a)$ remains to be determined. A likely candidate is the phosphorylation of CheB, but we note that straightforward mechanistic assumptions, such as a linear, hyperbolic, or quadratic dependence of [CheB-P] on a would not suffice to produce the observed sharp increase of $V_B(a)$ as a approaches

unity. Future experiments with phosphorylation-deficient mutants could shed light on this issue.

Noise and feedback dynamics near steady state

Single-cell measurements of motor output (Korobkova *et al*, 2004) have established that the steady-state activity of the *E. coli* chemotaxis pathway exhibits large fluctuations over a slow timescale. Through theoretical modeling and simulations, Emonet and Cluzel (2008) have argued that this could be attributable to the adaptation enzymes CheR and CheB operating near saturation, a phenomenon related to zero-order ultrasensitivity of reversible covalent-modification systems (Goldbeter and Koshland, 1981). Our data provide an experimental test for this hypothesis, as the biochemical parameters inferred from the above analysis of $F(a)$ can be used to assess the degree of saturation of the *in vivo* adaptation kinetics, and, in turn, the steady-state noise.

The values we obtained above of the Michaelis constants, K_R and K_B, and the pre-stimulus kinase-activity a_0, imply that $> \sim 70\%$ of both CheR and CheB are bound to their receptor substrates at steady state. Here, we apply the stochastic analysis of Emonet and Cluzel (2008) to our biochemical model for the adaptation system (equation (4) of the main text), to estimate the steady-state noise expected for kinase activity *in vivo*. The feedback transfer function $F(a)$ determines the dynamics of the adaptation system through equation (1). In the absence of chemical stimuli, the pathway activity, in turn, is determined completely by the adaptation system; by taking the time derivative of equation (2) and substituting into this equation (1), we find $\frac{da}{dt} = \frac{da}{dm} \frac{dm}{dt} = \alpha N a_0 (1 - a_0) F(a)$. Applying this result to the stochastic time-evolution equation obtained by Emonet and Cluzel (2008) by the 'linear noise approximation', the displacement from the steady-state activity, $\Delta a(t) = a(t) - a_0$, evolves in time as

$$\frac{d\Delta a(t)}{dt} = -\tau_a^{-1} \Delta a(t) + \sqrt{D} \eta(t) \qquad (5)$$

where $\tau_a = (-\alpha N a_0 (1 - a_0) F'(a_0))^{-1}$ is the relaxation time of the receptor–kinase-activity a, $\eta(t)$ represents temporally uncorrelated white noise, and $D = \left(\frac{da}{dm}\right)^2 / N_{tot} (V_R \frac{1 - a_0}{1 - a_0 + K_R} + V_B(a_0) \frac{a_0}{a_0 + K_B})$ is the strength of noise originating from the discrete methylation events occurring in N_{tot} receptor complexes. Computing the value of the relaxation time constant τ_a using the parameters a_0, $F'(a_0)$, N and α from our measurements, we obtain $\tau_a \approx 29$ s at 22°C and $\tau_a \approx 11$ s at 32°C. The solution for the amplitude of the steady-state fluctuations, σ_a, in the Emonet–Cluzel model (equation (5)) is $\sigma_a = \sqrt{\tau_a D / 2}$. With parameters for the CheR/CheB reactions inferred from our measured profile of $F(a)$, and assuming $N_{tot} = 10^4 / N$ (i.e. partitioning the $\sim 10^4$ receptor dimers in each cell into MWC clusters of size N), we obtain $\sigma_a / a_0 \approx 0.087$ at 22°C and $\sigma_a / a_0 \approx 0.077$ at 32°C.

Thus, our results are consistent with slow steady-state fluctuations in kinase activity, with a large amplitude of around $\sim 10\%$ of the mean and relaxation time constants in the range ~ 10–30 s. In an analysis of the noise-spectral data obtained by Korobkova *et al* (2004), Tu and Grinstein (2005)

found that intracellular [CheY-P] fluctuations must be both slow (the correlation time, $\tau_a \geqslant 1\,\mathrm{s}$) and of large amplitude ($>20\%$ of the mean) to explain the power-law dwell-time distribution in motor switching, as well as the $1/f$ noise observed in the switching-time power spectrum. According to the above analysis, the requirement for long correlation times (i.e. large τ_a) is clearly satisfied. Although the calculated noise amplitudes seem to fall somewhat short, we note that we have estimated these values from population measurements. Given the natural variation in protein levels between individual cells, we would expect the reported $1/f$ behavior to be measurable in some fraction of the population.

Concluding remarks

In this study, we have viewed the chemotaxis-signaling pathway as a signal processor, and characterized its performance by two phenomenological observables: the 'gradient sensitivity,' a quantity we defined using the constant activity reached by the pathway during exponential ramp stimuli (Figures 3A and 5A), and the frequency response, described here by the amplitude and phase of the response to exponential sine waves (Figures 4 and 5C). Calibration of the allosteric MWC model for the receptor module using step stimuli (Figure 7) revealed a linear dependence of receptor-free energy on the level of covalent modification. This finding admitted a particularly simple solution to our pathway model (equations (1) and (2)), in which the gradient sensitivity depends on the way in which the adaptation and receptor modules are coupled *in vivo* (through the function $F(a)$ of the adaptation module and the parameter α of the receptor module), but not explicitly on receptor cooperativity (the parameter N of the receptor module). The frequency response, however, depends also on the degree of receptor cooperativity (both the cutoff frequency for time-derivative computations and the amplitude are proportional to N).

Although the ramp-response data allowed us to deduce the underlying chemical kinetics of the adaptation enzymes (Figures 3B and 5B), we note that the frequency response, with its dependence on N, is relevant in considering the chemotactic performance of bacteria executing spatial searches in the real world. Swimming bacteria execute random walks by a run/tumble mechanism (Berg and Brown, 1972) to convert spatial gradients of chemoeffectors into temporal ones. In such searches, time-derivative computations must be made while swimming direction is being randomized. Thus, the sensitivity to sustained temporal ramps cannot be directly interpreted as the sensitivity of swimming cells to spatial gradients. The frequency response is more relevant in considering this problem, as we can view the input fluctuations because of randomized swimming as additional 'noise' with its characteristic frequency spectrum (determined by the statistics of tumbling and rotational Brownian motion). The question of how such noise arising from random motility is filtered during spatial searches has been addressed implicitly in a number of recent studies, in which numerical simulations were used to predict the migratory behavior of bacterial populations with different adaptation time scales (Andrews *et al*, 2006; Bray *et al*, 2007; Emonet and Cluzel, 2008; Jiang *et al*, 2010). Our measurements and analyses of the frequency

response reported here provide a firm grounding for further analytical treatments of this problem (Sartori and Tu, submitted). Viewed as a signal filter, a crucial characteristic of the frequency response is the cutoff frequency, ν_m, below which time-derivative sensing can occur. As $\nu_m \propto NF'(a_0)$, the receptor cooperativity N can have a buffering function in keeping ν_m reasonably high when adaptation feedback is weak (i.e. when the value of $F'(a_0)$ is small).

Another important source of noise in chemotactic signaling, namely that due to fluctuations in the intracellular concentrations of signaling species, could be addressed directly by our current findings. The relatively slow relaxation times we obtained for the pathway activity near steady state provide support for the view that the large-amplitude fluctuations observed by Korobkova *et al* (2004) could originate in the attenuated feedback near steady state (i.e. small $F'(a_0)$) resulting from enzyme saturation. This result also highlights the importance of using dynamically modulated stimuli to probe the adaptation kinetics near steady state—the often used strategy of linearly interpolating between the limiting adaptation kinetics measured during large step responses ($F(0)$ and $F(1)$ in our model) would have provided a very different estimate for $F'(a_0)$, and hence the relaxation time. Moreover, our data and analysis make clear that the strength of feedback affects not only the steady-state fluctuations, but also the gradient sensitivity and frequency response of the pathway, as evidenced by measurements at two temperatures (Figure 5). It is then reasonable to expect that the pathway's relaxation time scale, which could be tuned by the expression level or kinetic parameters of CheR and CheB, is under selective pressure for its effects on gradient-sensing parameters such as the cutoff frequency for time-derivative computations, in addition to its effects on the steady-state noise.

Materials and methods

Strains and plasmids

All bacterial strains used in this study were derivatives of *E. coli* K12 strain AW405 (Armstrong *et al*, 1967). VS104 is a *cheYcheZ* mutant (Sourjik and Berg, 2002b) of a widely studied AW405 derivative, RP437 (Parkinson and Houts, 1982). TSS178 is an analogous *cheYcheZ* mutant of the parent strain AW405, constructed for this study. For the step-response measurements to calibrate the receptor-module transfer function, G, we used Tsr− Tap− CheR− CheB− derivatives of VS104 in which the *tar* receptor gene is mutated at its covalent-modification sites (gifts of V Sourjik). The identity of these strains were, in order of increasing amidation levels, VS144 (EEEE), VS141 (QEEE), VS148 (QEQE), VS150 (QEQQ), SB1 (QQQQ). The strain VS178 is Tsr− Tap−, but retains the wild-type *cheR* and *cheB* genes. Plasmid pVS113 encodes the cheR gene under the control of an arabinose-inducible promoter, and plasmid pVS88 encodes the fluorescent fusion proteins CheY-YFP and CheZ-CFP under control of an isopropyl β-D-thio-galactopyranoside-inducible promoter (Sourjik and Berg, 2004).

In vivo FRET measurements and data analysis

FRET microscopy of bacterial populations were carried out essentially as described earlier (Sourjik *et al*, 2007). The FRET donor–acceptor pair was CheZ-CFP and CheY-YFP, expressed from a plasmid in strain backgrounds that lack the native copies of the *cheY* and *cheZ* genes. Cells attached to poly-L-lysine-treated microscope coverslips were seated at the top face of a flow cell (Berg and Block, 1984). The microscope was a Nikon TE300 equipped with a PlanFluor $\times 40$ 0.50

n.a. objective. The sample was illuminated by a 75 W super quiet xenon lamp (Hamamatsu, Bridgewater, NJ) through an excitation bandpass filter (Semrock FF01-438/24-25) and a dichroic mirror (Semrock FF458-Di01-25 × 36), and epifluorescent emission was further split into donor (cyan, *C*) and acceptor (yellow, *Y*) channels by a second dichroic mirror (Chroma 515DCXR) and collected through emission bandpass filters (Semrock FF01-483/32-25 and FF01-542/27) by photon-counting photomultipliers (Hamamatsu H7421-40).

Signal intensities of the acceptor and donor channels were recorded by a computer running LabView (National Instruments), and the ratio between the two channels ($R=Y/C$) provided an indicator of FRET activity that is robust to fluctuations in excitation intensity. The change in FRET efficiency, ΔFRET, can be computed at every time point from the recorded data using the ratio change $\Delta R_S \equiv (R - R_{pre})$ as $\Delta\text{FRET} = (R_{pre} + \Delta R_S - R_0)/(R_{pre} + \Delta R_S + |\Delta Y/\Delta C|) - (R_{pre} - R_0)/(R_{pre} + |\Delta Y/\Delta C|)$, where R_0 is the acceptor-to-donor ratio in the absence of FRET, R_{pre} is pre-stimulus ratio of acceptor- to donor-channel intensities (measured either in the absence of attractant, or after adapting to a constant value of $[L]$), and $|\Delta Y/\Delta C|$ is the (constant) absolute ratio between the changes in the acceptor- and donor-channel signals per FRET pair (Sourjik *et al*, 2007). Under the conditions of the measurements performed here, however, backgrounds in the *Y* and *C* channels were negligible, R_{pre} and $|\Delta Y/\Delta C|$ were practically constant, and we found consistently that $R_{pre} + |\Delta Y/\Delta C| \gg \Delta R_S$. Thus, $\Delta\text{FRET} \approx \Delta R_S/(R_{pre} + |\Delta Y/\Delta C|)$ was essentially proportional to ΔR_S (worst case nonlinearity ~3%) and comparable between measurements. We, therefore, expressed ΔFRET, for simplicity, in arbitrary units of ΔR_S throughout this study.

MWC model for the receptor module $G([L], m)$

In this study, we use a calibrated allosteric model of the receptor module, *G*. The shape of *G* has been mapped in detail in recent *in vivo* FRET experiments of kinase activity through dose–response measurements using step stimuli. This function characterizes the response of the receptor–kinase complex in Figure 1A, taking as input $[L]$ and *m* to yield the output *a*. Much recent work has shown this function to be well approximated by a two-state model,

$$G([L], m) = \frac{1}{1 + e^{f_t([L], m)}} \tag{6}$$

wherein the total free-energy difference between the two output states, f_t, is simply proportional to the sum of ligand-dependent and modification-dependent parts:

$$f_t([L], m) = N(f_L([L]) + f_m(m)) \tag{7}$$

When the parameter *N* is an integer greater than unity, it can be interpreted as the number of ligand-binding subunits in an oligomeric complex with tightly coupled output (i.e. their activity transitions are concerted so that the collective output has only two states), and is equivalent to the MWC model of allostery (Monod *et al*, 1965). An important assumption of the model is that the ligand dissociation constant for binding sites depends on the activity state of the oligomer. This leads to a simple analytical form for the ligand-dependent free energy per ligand-binding subunit, f_L:

$$f_L([L]) = \ln\left[\frac{1 + [L]/K_I}{1 + [L]/K_A}\right] \tag{8}$$

where K_A and K_I are the ligand dissociation constants for the active and inactive states of the oligomer, respectively. The model does not specify the functional form of the modification-dependent free energy, $f_m(m)$, but this can be determined experimentally by fitting the MWC model (equations (6)–(8)) to dose–response curves of kinase activity. *In vivo* FRET experiments, which measured the response of the aspartate receptor Tar when stimulated by the attractant MeAsp yielded a linear form for f_m:

$$f_m(m) = -\alpha(m - m_0) \tag{9}$$

where α is the free-energy change per added methyl group (Figure 7); we note that these measurements were made at room temperature, that is ~22°C. With $N=6$ and $K_I/K_A=0.0062$, α was found to have a value ~2 kT, and the crossover methylation level, m_0 (defined as the

methylation level at which $f_m(m)=0$) was found to be ~0.5. This calibration of the function *G* provides the basis for our strategy to probe the adaptation module of the pathway through the receptor module, as it establishes the quantitative relationship between effects of methylation and ligand concentration on kinase output, which we monitor by FRET.

Input–output measurements by FRET

We used three classes of time-varying stimuli to probe the transfer functions of the chemotaxis system. Step stimuli were used to characterize the function $G([L], m)$ for the Tar receptor in an array of Tsr− Tap− CheR− CheB− mutants with fixed receptor-modification states. As these cells lack the receptor-modifying enzymes CheR and CheB, the input–output relation of the receptor module can be measured in an open-loop configuration, without adaptation feedback. The lack of the Tsr and Tap receptors renders the Tar receptor the dominant majority in the remaining receptor population. In this genetic background, step responses to rapid changes in [MeAsp] were measured in 'modification-standard strains' bearing various point mutations at the four modification sites of the Tar receptor, corresponding to the EEEE, QEEE, QEQE, QEQQ, and QQQQ modification states (in which the four-letter code denotes the state of the amino-acid residue at the four modification sites; 'E' signifies a glutamate, and 'Q' a glutamine). As the glutamine (Q) residues differ in their chemical structure from a glutamate (E) only by the addition of an amide group, E→Q substitution mutations have long been used as an experimental proxy for studying the effects of the more biologically relevant methylated glutamate residues (Em), which cannot be encoded genetically. Here, we also studied the effect of Em modifications by overexpressing CheR from a plasmid in the same 'modification-standard strains,' thus yielding, in addition to the above, the modification states QEmQQ, QEmQEm, QEmEmEm, and EmEmEmEm. Dose–response data were collected for strains representing these nine states, and for Tsr− Tap− CheR+ CheB+ cells (Figure 7A). Fitting of these data to the MWC model (see Materials and methods) yielded estimates, in units of free energy, of how strongly each added Q- or Em-modification affects the activity of the Tar receptor (Figure 7B). We found that Em-modifications have an ~2.5-fold stronger effect than Q-modifications.

We then used exponential ramp stimuli to probe the shape of the feedback transfer function $F(a)$ (equation (1)). The main idea of the measurement hinges on the observation by Block *et al* (1983) that the pathway output reaches a constant value during exponential ramps of the form $[L](t)=[L]_0 e^{rt}$ (Figure 2A and B). Within our MWC model of the receptor module, the dependence of kinase activity on the total free-energy f_t is monotonic (equation (6)). Therefore, as the activity $a(t)$ approaches a constant, so does the free energy, that is

$$\frac{df_t}{dt} = N\left[\frac{df_L}{dt} + \frac{df_m}{dt}\right] \to 0, \quad \text{as} \quad \frac{da(t)}{dt} \to 0 \tag{10}$$

In our calibrated MWC model (the function $G([L],m)$ in equation (2)), the ligand-dependent free energy, $f_L([L])$ (equation (8)), possesses a broad (~2.5 orders of magnitude) domain in its input ligand concentration $[L]$ over which f_L is essentially linear in $\ln[L]$. This implies that an exponential ramp that operates within this range ($K_I \ll [L] \ll K_A$) at rate *r* will cause a constant change in f_L per unit time, at precisely the same ramp rate *r* (i.e. $f_L(t)=rt$). On the other hand, our receptor-model calibration also obtained a linear relationship between the modification-dependent portion of free energy, $f_m(m)$, and the methylation level, *m* (equation (9)), so combined with our model for the rate of change of methylation (equation (1)), the methylation-dependent free energy follows $f_m(t)=-\alpha F(a)t$. Combining these with the constancy condition for the total free energy (equation (10)), we obtain a simple relationship between the applied ramp rate *r* and the *in vivo* feedback transfer function $F(a)$ during exponential ramps,

$$r = \alpha F(a_c) \tag{11}$$

Thus, by controlling the input, *r* while measuring the constant output, a_c the functional form of $F(a)$ can be mapped by plotting r/α against the measured values of a_c.
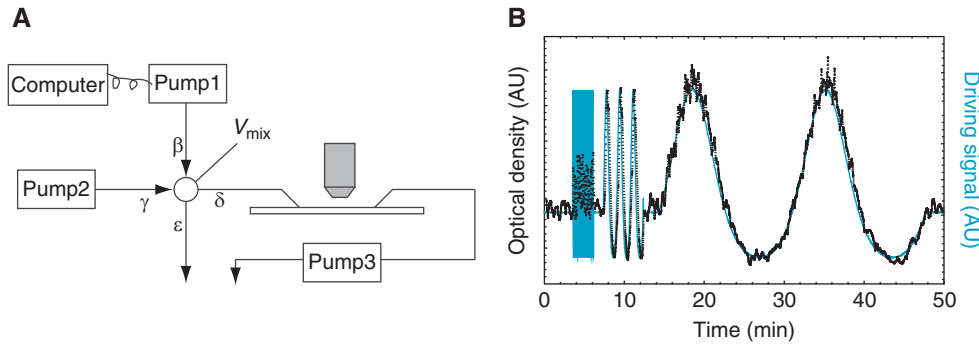
Figure 8 Chemical waveform generator: design and performance. (**A**) The chemical waveform generator, based on the design of Block *et al* (1983). A mixing chamber of volume V_{mix} was fed two inputs: attractant at a high concentration at computer-controlled rate β and buffer at rate γ. The output concentration $[L]$, seen by cells in the flow cell, perfused at rate δ, was proportional to the rate β, provided that $\gamma \gg \beta$. Under these conditions, the time for mixing, τ_{mix}, was fixed at V_{mix}/γ. Thus, by programming the pump controlling β, arbitrary waveforms could be generated as a function of time. In our experiments, $V_{mix} \approx 120\,\mu l$ and $\gamma > 1200\,\mu l/min$, so τ_{mix} was $< 6\,s$. The rate δ does not affect τ_{mix}, but affects the exchange time τ_{ex} of fluid in the flow cell and the polyethylene tubing connecting it to the mixing chamber, so this was also kept relatively high ($\sim 1000\,\mu l/min$). (**B**) We confirmed, by measuring the optical density of bromothymol blue (black points), that temporal gradients of arbitrary function could be programmed (blue curve) provided that the frequency of the programmed signal did not exceed the mixing frequency $\nu_{mix} = (2\pi\tau_{mix})^{-1}$. This condition was violated for the blue segment at the left end of the plot.

The third class of input–output measurements we performed involved measuring the response in kinase activity to exponential sine-wave stimuli of the form $[L](t) = [L]_0 e^{A_L \sin(2\pi\nu t)}$ (Figure 4A). The response was always found to be sinusoidal, $a(t) = a_0 + |A|\cos(2\pi\nu t - \varphi_D)$ where the frequency ν (in Hz) always matched that of the input, as expected for a linear system. We can solve for both the response amplitude $|A|$ and phase delay φ_D in our model by linearizing equations (1) and (2). This gives

$$A = \frac{i\nu N a_0 (1 - a_0)}{i\nu + \nu_m} A_L \tag{12}$$

$$|A| = \frac{N a_0 (1 - a_0)}{\sqrt{1 + (\nu_m/\nu)^2}} A_L \tag{13}$$

for the response amplitude, and

$$\phi_D = \pi - \tan^{-1}(\nu_m/\nu) \tag{14}$$

for the phase delay, where in equations (12)–(14), $\nu_m = -\alpha N a_0 (1 - a_0) F'(a_0)/2\pi$ defines a characteristic frequency determined by the adaptation kinetics and receptor parameters. Considering the two limits of equation (12), $\phi_D \to \pi$ for $\nu \gg \nu_m$ and $\phi_D \to \pi/2$ for $\nu \ll \nu_m$, makes it clear that ν_m delineates the range of possible input frequencies ν into two regimes: below ν_m, the system takes the time derivative of the input (i.e. the output is 90° out of phase), whereas above ν_m, the system simply follows the input in phase (although the output seems 180° out of phase, because of the negative response of kinase activity to attractant). Finally, by taking the Fourier transform of the signal's time derivative $B \equiv \int \frac{d[L]}{dt} e^{-2\pi i \nu t} dt = i\nu A_L$ and factoring this out from the general solution (equation (12)), we obtain the system's time-derivative-filtering function

$$H \equiv A/B = \frac{N a_0 (1 - a_0)}{i\nu + \nu_m} \tag{15}$$

The absolute value of this function, $|H|$, plotted in Figure 4B, clarifies the low-pass-filtering properties of the chemotaxis pathway for the input signal's time derivative.

Dynamic modulation of chemoeffector stimuli

Control of the temporal profile of attractant stimulus was achieved by a mixing apparatus (Figure 8A), based on the design of Block *et al* (1983). The mixing chamber was a cylinder fabricated of Delrin, with an internal volume $V_{mix} \approx 100\,\mu l$, with two input channels (β and γ) and two output channels (δ and ε). The rate of attractant delivery, β, at concentration $[L]_\beta$, by a syringe pump (Harvard Apparatus

PHD 22/2000) was controlled through the same LabView program collecting the data to facilitate input/output comparisons. A peristaltic pump (Rainin Rabbit) pushed buffer into the chamber through the other input channel at a constant rate, γ. Negative pressure was applied to both output channels of the mixer, the first by a peristaltic-pump pulling fluid at a constant rate, δ, through the flow cell, and the second by a gravity-induced hydrostatic force (applied by lowering the height at which the outlet of the connected tubing rested), which pulled fluid to drain at a rate ε. When β is constant, the output concentration $[L](t)$ approaches $[L]_\infty = [L]_\beta \beta/(\beta + \gamma)$ as $[L](t) = [L]_\infty + ([L]_0 - [L]_\infty)e^{-t/\tau_{mix}}$, where $[L]_0$ is the initial concentration and $\tau_{mix} \equiv V_{mix}/(\beta + \gamma)$. In all of our experiments, we set $\gamma \gg \beta$ so that $[L]_\infty \approx [L]_\beta \beta/\gamma$ and $\tau_{mix} \approx V_{mix}/\gamma$. Thus, when β is dynamic, $[L](t)$ is proportional to β as long as the latter is varied smoothly over time scales much longer than τ_{mix} (Figure 8B).

Supplementary information

Supplementary information is available at the *Molecular Systems Biology* website (www.nature.com/msb).

Conflict of interest

The authors declare that they have no conflict of interest.

References

Alon U (2007) *An Introduction to Systems Biology*. Boca Raton, FL: CRC Press

Alon U, Surette MG, Barkai N, Leibler S (1999) Robustness in bacterial chemotaxis. *Nature* **397:** 168–171

Andrews BW, Yi TM, Iglesias PA (2006) Optimal noise filtering in the chemotactic response of *Escherichia coli*. *PLoS Comput Biol* **2:** e154

Antommattei FM, Munzner JB, Weis RM (2004) Ligand-specific activation of *Escherichia coli* chemoreceptor transmethylation. *J Bacteriol* **186:** 7556–7563

Armstrong JB, Adler J, Dahl MM (1967) Nonchemotactic mutants of *Escherichia coli*. *J Bacteriol* **93:** 390–398

Barkai N, Leibler S (1997) Robustness in simple biochemical networks. *Nature* **387:** 913–917

Bennett MR, Pang WL, Ostroff NA, Baumgartner BL, Nayak S, Tsimring LS, Hasty J (2008) Metabolic gene regulation in a dynamically changing environment. *Nature* **454:** 1119–1122

Berg HC, Block SM (1984) A miniature flow cell designed for rapid exchange of media under high-power microscope objectives. *J Gen Microbiol* **130:** 2915–2920

Berg HC, Brown DA (1972) Chemotaxis in Escherichia coli analysed by three-dimensional tracking. *Nature* **239:** 500–504

Berg HC, Tedesco PM (1975) Transient response to chemotactic stimuli in *Escherichia coli*. *Proc Natl Acad Sci USA* **72:** 3235–3239

Block SM, Segall JE, Berg HC (1983) Adaptation kinetics in bacterial chemotaxis. *J Bacteriol* **154:** 312–323

Boldog T, Grimme S, Li M, Sligar SG, Hazelbauer GL (2006) Nanodiscs separate chemoreceptor oligomeric states and reveal their signaling properties. *Proc Natl Acad Sci USA* **103:** 11509–11514

Borczuk A, Staub A, Stock J (1986) Demethylation of bacterial chemoreceptors is inhibited by attractant stimuli in the complete absence of the regulatory domain of the demethylating enzyme. *Biochem Biophys Res Commun* **141:** 918–923

Borkovich KA, Alex LA, Simon MI (1992) Attenuation of sensory receptor signaling by covalent modification. *Proc Natl Acad Sci USA* **89:** 6756–6760

Bornhorst JA, Falke JJ (2001) Evidence that both ligand binding and covalent adaptation drive a two-state equilibrium in the aspartate receptor signaling complex. *J Gen Physiol* **118:** 693–710

Bray D (1998) Signaling complexes: biophysical constraints on intracellular communication. *Annu Rev Biophys Biomol Struct* **27:** 59–75

Bray D, Levin MD, Lipkow K (2007) The chemotactic behavior of computer-based surrogate bacteria. *Curr Biol* **17:** 12–19

Cluzel P, Surette M, Leibler S (2000) An ultrasensitive bacterial motor revealed by monitoring signaling proteins in single cells. *Science* **287:** 1652–1655

Duke TA, Bray D (1999) Heightened sensitivity of a lattice of membrane receptors. *Proc Natl Acad Sci USA* **96:** 10104–10108

Dunten P, Koshland Jr DE (1991) Tuning the responsiveness of a sensory receptor via covalent modification. *J Biol Chem* **266:** 1491–1496

Emonet T, Cluzel P (2008) Relationship between cellular response and behavioral variability in bacterial chemotaxis. *Proc Natl Acad Sci USA* **105:** 3304–3309

Endres RG, Oleksiuk O, Hansen CH, Meir Y, Sourjik V, Wingreen NS (2008) Variable sizes of *Escherichia coli* chemoreceptor signaling teams. *Mol Syst Biol* **4:** 211

Goldbeter A, Koshland Jr DE (1981) An amplified sensitivity arising from covalent modification in biological systems. *Proc Natl Acad Sci USA* **78:** 6840–6844

Hartwell LH, Hopfield JJ, Leibler S, Murray AW (1999) From molecular to modular cell biology. *Nature* **402:** C47–C52

Hersen P, McClean MN, Mahadevan L, Ramanathan S (2008) Signal processing by the HOG MAP kinase pathway. *Proc Natl Acad Sci USA* **105:** 7165–7170

Jiang L, Ouyang Q, Tu Y (2010) Quantitative modeling of *Escherichia coli* chemotactic motion in environments varying in space and time. *PLoS Comput Biol* **6:** e1000735

Kalinin YV, Jiang L, Tu Y, Wu M (2009) Logarithmic sensing in *Escherichia coli* bacterial chemotaxis. *Biophys J* **96:** 2439–2448

Keymer JE, Endres RG, Skoge M, Meir Y, Wingreen NS (2006) Chemosensing in *Escherichia coli*: two regimes of two-state receptors. *Proc Natl Acad Sci USA* **103:** 1786–1791

Korobkova E, Emonet T, Vilar JM, Shimizu TS, Cluzel P (2004) From molecular noise to behavioural variability in a single bacterium. *Nature* **428:** 574–578

Lai RZ, Manson JM, Bormans AF, Draheim RR, Nguyen NT, Manson MD (2005) Cooperative signaling among bacterial chemoreceptors. *Biochemistry* **44:** 14298–14307

Li G, Weis RM (2000) Covalent modification regulates ligand binding to receptor complexes in the chemosensory system of *Escherichia coli*. *Cell* **100:** 357–365

Mello BA, Shaw L, Tu Y (2004) Effects of receptor interaction in bacterial chemotaxis. *Biophys J* **87:** 1578–1595

Mello BA, Tu Y (2003) Quantitative modeling of sensitivity in bacterial chemotaxis: the role of coupling among different chemoreceptor species. *Proc Natl Acad Sci USA* **100:** 8223–8228

Mello BA, Tu Y (2005) An allosteric model for heterogeneous receptor complexes: understanding bacterial chemotaxis responses to multiple stimuli. *Proc Natl Acad Sci USA* **102:** 17354–17359

Mello BA, Tu Y (2007) Effects of adaptation in maintaining high sensitivity over a wide range of backgrounds for *Escherichia coli* chemotaxis. *Biophys J* **92:** 2329–2337

Mettetal JT, Muzzey D, Gomez-Uribe C, van Oudenaarden A (2008) The frequency dependence of osmo-adaptation in *Saccharomyces cerevisiae*. *Science* **319:** 482–484

Monod J, Wyman J, Changeux JP (1965) On the nature of allosteric transitions: a plausible model. *J Mol Biol* **12:** 88–118

Parkinson JS, Houts SE (1982) Isolation and behavior of *Escherichia coli* deletion mutants lacking chemotaxis functions. *J Bacteriol* **151:** 106–113

Segall JE, Block SM, Berg HC (1986) Temporal comparisons in bacterial chemotaxis. *Proc Natl Acad Sci USA* **83:** 8987–8991

Shi Y, Duke T (1998) Cooperative model of bacterial sensing. *Phys Rev E* **58:** 6399–6406

Shimizu TS, Aksenov SV, Bray D (2003) A spatially extended stochastic model of the bacterial chemotaxis signalling pathway. *J Mol Biol* **329:** 291–309

Skoge ML, Endres RG, Wingreen NS (2006) Receptor-receptor coupling in bacterial chemotaxis: evidence for strongly coupled clusters. *Biophys J* **90:** 4317–4326

Sourjik V, Berg HC (2002a) Binding of the *Escherichia coli* response regulator CheY to its target measured *in vivo* by fluorescence resonance energy transfer. *Proc Natl Acad Sci USA* **99:** 12669–12674

Sourjik V, Berg HC (2002b) Receptor sensitivity in bacterial chemotaxis. *Proc Natl Acad Sci USA* **99:** 123–127

Sourjik V, Berg HC (2004) Functional interactions between receptors in bacterial chemotaxis. *Nature* **428:** 437–441

Sourjik V, Vaknin A, Shimizu TS, Berg HC (2007) *In vivo* measurement by FRET of pathway activity in bacterial chemotaxis. *Methods Enzymol* **423:** 363–391

Spudich JL, Koshland Jr DE (1975) Quantitation of the sensory response in bacterial chemotaxis. *Proc Natl Acad Sci USA* **72:** 710–713

Tu Y, Grinstein G (2005) How white noise generates power-law switching in bacterial flagellar motors. *Phys Rev Lett* **94:** 208101

Tu Y, Shimizu TS, Berg HC (2008) Modeling the chemotactic response of *Escherichia coli* to time-varying stimuli. *Proc Natl Acad Sci USA* **105:** 14855–14860

Yi TM, Huang Y, Simon MI, Doyle J (2000) Robust perfect adaptation in bacterial chemotaxis through integral feedback control. *Proc Natl Acad Sci USA* **97:** 4649–4653